Macedonian Journal of Chemistry and Chemical Engineering, Vol. **38**, No. 1, pp. 49–62 (2019)

MJCCA9 – 768

ISSN 1857-5552
e-ISSN 1857-5625

Received: November 4, 2017
Accepted: February 12, 2019

DOI: 10.20450/mjcce.2019.1333
Original scientific paper

STRUCTURAL CHARACTERIZATION OF KAEMPFEROL: A SPECTROSCOPIC AND COMPUTATIONAL STUDY

Dejan Milenković[1*], Jasmina M. Dimitrić Marković[2], Dušan Dimić[2], Svetlana Jeremić[3], Dragan Amić[4], Marijana Stanojević Pirković[5], Zoran S. Marković[3]

[1]Bioengineering Research and Development Center, 34000 Kragujevac, Republic of Serbia
[2]Faculty of Physical Chemistry, University of Belgrade, Studentski trg 12–16, 11000 Belgrade, Republic of Serbia
[3]Department of Chemical-Technological Sciences, State University of Novi Pazar, Vuka Karadžića bb, Novi Pazar, 36300, Republic of Serbia
[4]Faculty of Agriculture, Josip Juraj Strossmayer University of Osijek, Kralja Petra Svačića 1D, 31000 Osijek, Republic of Croatia
[5]Faculty of Medical Sciences University of Kragujevac, Svetozara Markovića 69, 34000 Kragujevac, Serbia

deki82@kg.ac.rs

Calculations based on the density functional theory, with the B3LYP functional and the 6-311++G(d,p) basis set, were performed with the aim of confirming the molecular structure and spectroscopic characteristics of kaempferol, a naturally occurring flavonoid molecule. The electronic structure of kaempferol was examined using NBO analysis. The assigning of the experimentally obtained IR and Raman spectra was performed after the best-fit-based comparison with theoretical spectra. The ^{13}C and ^{1}H NMR experimental spectra were related to the theoretically obtained values of the chemical shifts determined by the GIAO method. The correlation coefficient and the average absolute error values proved B3LYP-D3 to be an adequate method in describing the NMR parameters of kaempferol. Molecular docking analysis was carried out in order to identify the potency of inhibition of the title molecule against human procalcitonin. The inhibition activity was obtained for 10 conformations of ligand inside the protein.

Keywords: kaempferol; density functional theory; spectroscopic characterization; molecular docking

СТРУКТУРНА КАРАКТЕРИЗАЦИЈА НА КАМФЕРОЛ: СПЕКТРОСКОПСКИ И КОМПЈУТЕРСКИ ИСПИТУВАЊА

Извршени се пресметки базирани на теоријата на густина на функционалот со функционалот B3LYP и основниот сет 6-311++G(d,p) со цел да се потврдат молекулската структура и спектроскопските карактеристики на камферол, флавоноидна молекула од природно потекло. Електронската структура беше испитана со NBO анализа. Асигнацијата на експериментално добиените IR и рамански спектри беше извршена со најдобро усогласената споредба со теоретските спектри. Експерименталните спектри ^{13}C и ^{1}H NMR беа споредени со теоретски добиените вредности на хемиските поместувања определени со методот GIAO. Коефициентот на корелација и просечните вредности на апсолутната грешка покажаа дека B3LYP-D3 е соодветен метод за опишување на NMR-параметрите на камферол. Анализата на припојување беше извршена со цел да се идентификува способноста за инхибиција на ова соединение со хуман прокалцитонин. Инхибициската активност беше добиена за 10 конформации на лигандот внатре во протеинот.

Клучни зборови: камферол; теорија на густина на функционалот; спектроскопско молекулско припојување

1. INTRODUCTION

Flavonoids, as natural polyphenolic compounds, are reported to exert a wide range of positive health effects arising mainly from their antioxidant ability. They represent an important group of phytochemicals with over 8000 individual compounds known. They have roles as antioxidants, antimicrobials, receptors and screening molecules for light, visual attractors and feeding repellents. Flavonoids are common in everyday human diet, as their presence indicates good-quality food, flavor identification, and taste thresholds influencing food preference [1, 2]. The fact that flavonoids are recognized as highly potent external defense components against oxidative stress in various stages, makes them some of the most widely investigated biochemically active molecules today [3].

Many studies on flavonoids have shown that they exhibit prominent therapeutic and pharmacological activities, among which their antiallergenic, antiviral, anti-inflammatory and vasodilating properties are particularly interesting. Most studies into antioxidant activity are related to their structural features: the carbon–carbon double bond in position 2, an OH group in position 3, OH groups present in the A and B rings, and AC–B ring coplanarity [4–16]. However, it has been found that, under the specific conditions, some can exhibit prooxidant activity as well [12].

Kaempferol (3,5,7-trihydroxy-2-(4'-hydroxyphenyl)-4*H*-chromen-4-one; Fig. 1) is a natural flavonoid that can be found mainly in vegetables (broccoli, cabbage, leek, beans, tomato), fruits (strawberries, grapes), tea, gingko, and in many medical herbs used in traditional medicine [3, 17]. Known as a strong antioxidant, kaempferol helps in the prevention of arteriosclerosis, inhibits the oxidation of low-density lipoproteins and lowers the aggregation of platelets in the blood. It reduces the risk of cancer development (including pancreatic, lung and gastric cancer and ovarian cancer in women) by inhibiting angiogenesis in vitro and/or in vivo [3]. Kaempferol has proven its pharmacological activity as good radical scavenger in patients with diabetes, asthma and carcinogenesis [18]. It also inhibits enzymes such as cyclooxygenases (COXs), lipoxygenases (LOXs), and induces nitric oxide synthase (iNOS) known to be present during the process of inflammation [3].

Numerous authors characterize an investigated compound by comparing theoretical and experimental results [19–21]. The aim of this study is to contribute to the elucidation of the structure of kaempferol by using quantum chemical calculations at the B3LYP-D3 level of theory in conjunction with different spectroscopic methods (IR, Raman and ^{1}H and ^{13}C NMR).

In addition, kaempferol is investigated for its reactivity toward human procalcitonin (PCT) protein by means of molecular docking analysis. PCT (~13 kDa) is a peptide consisting of 116 amino acids. This protein is degraded enzymatically into lower-molecular-weight peptides. Calcitonin is the final product and consists of 32 amino acids. In the serum of healthy humans, all precursors can be detected, including PCT and the mature peptide hormone. In septic patients, the PCT in serum contains a peptide of only 114 amino, instead of the predicted PCT of 116 amino acids in healthy patients [22]. The biological effect of this protein was proven in the study of Nylén et al., who showed that the elevated concentrations can lead to sepsis, but can be treated by anti-PCT antibodies [23].

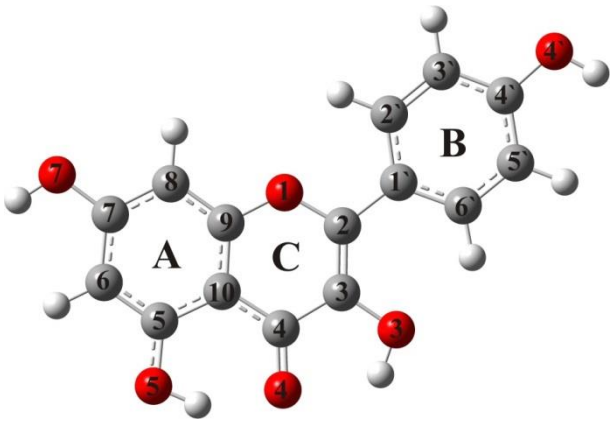

Fig. 1. The optimized structure and numbering of kaempferol

2. EXPERIMENTAL SECTION

2.1. *Materials*

Kaempferol and potassium bromide (KBr, IR grade) were obtained from Aldrich. Both chemicals were used without further purification.

2.2. *IR, Raman and NMR spectra*

The IR spectrum of kaempferol was recorded on a Thermo Nicolet 6700 FT-IR spectrometer equipped with ATR and DTGS TEC detectors. The experimental parameters were the following: spectral resolution 2 cm^{-1}, number of sample scans 512 and the number of background scans 512. The investigated molecule was studied in KBr matrix in a kaempferol/KBr ratio of 1:200. The IR spectrum was recorded in the 4000–400 cm^{-1} region. The

Raman spectrum was recorded on a Thermo Scientific DXR Raman spectrometer. The excitation source was a high-brightness diode-pumped solid-state laser with wavelength 532 nm. The objective lens was set to the value of 50 ×. A spectrograph with a 900 lines mm^{-1} grating was used for analysis of the scattered light. The spectrum was obtained between 3400 and 400 cm^{-1} directly from the pure powder samples. The output of the laser was fixed at 10 mW with an acquisition time of 10 s with 10 scans. Fluorescence was corrected for, and data acquisition and processing was performed with Thermo Scientific OMNIC software.

The theoretical Raman intensities (I_i^R) were derived based on the Raman scattering activities:

$$I_i^R = C(\upsilon_0 - \upsilon_i)^4 \cdot \upsilon_i^{-1} \cdot B_i^{-1} \cdot S_i \qquad (1)$$

The quantity B_i is a temperature factor that includes the contribution of the excited vibrational states, as predicted by the Boltzmann distribution:

$$B_i = 1 - \exp\left(-\frac{h\upsilon_i c}{kT}\right) \qquad (2)$$

where *h*, *k*, *c* and T are the Planck and Boltzmann constants, the speed of light and temperature, respectively. The wavenumber of the laser excitation line is υ_0 (υ_0 = 18 797 cm^{-1} corresponding to 532 nm), υ_i is the wavenumber of the normal mode (cm^{-1}), while S_i is the Raman scattering activity of the normal mode Q_i. The calculated Raman intensity, I_i^R, is presented in arbitrary units (*C* is a constant equal to 10^{-12}). Because of the low contribution of the excited vibrational states, the value of B_i is assumed to be 1. Otherwise, as is reported in the literature, the calculated Raman intensities for the bands below 300 cm^{-1} were overestimated when compared to the experimental values [24].

NMR spectra, in DMSO-d6 with TMS as internal standard, were determined on a Varian Gemini 200 MHz NMR spectrometer (^{1}H at 200 MHz and ^{13}C at 50 MHz).

3. THEORETICAL BACKGROUND

Optimization of the geometry of kaempferol was performed by using a B3LYP-D3 local density functional method and the 6-311++G (d, p) basis set, as implemented in the Gaussian 09 package [25–28]. This functional has been successfully reported in the literature for similar compounds [29, 30]. B3LYP-D3 was selected as a method widely applied for the NMR chemical shifts of similar molecules that has proved to predict the interatomic interactions at short and medium distances (≤5 Å) more accurately and reliably than traditional DFT methods. Hybrid GGA B3LYP-D3 included an empirical correction term proposed by Grimme [31, 32] and the stability of the obtained structure was verified to be the minimum on the potential energy surface. The calculated wavenumbers were scaled by a factor of 0.9873 in order to obtain a better match between the calculated and the experimental wavenumber values. For the prediction of IR and Raman spectra, the optimized gas-phase geometry was used. PED (Potential Energy Distribution) analysis using VEDA software was applied for estimation and assignation of the vibrational modes [33. 34]. The ^{1}H and ^{13}C chemical shifts were predicted by means of the GIAO (Gauge Independent Atomic Orbital) method, as implemented in Gaussian 09 with DMSO as solvent [35]. The NBO analysis was performed by using NBO 5.9 software [36, 37]. The polarizability and hyperpolarizability tensors (α_{xx}, α_{xy}, α_{yy}, α_{xz}, α_{yz}, α_{zz} and β_{xxx}, β_{xxy}, β_{xyy}, β_{yyy}, β_{xxz}, β_{xyz}, β_{yyz}, β_{xzz}, β_{yzz}, β_{zzz}) can be obtained by a Gaussian frequency job output file. The molecular docking simulation was carried out using AutoDock 4.0 software [38]. The structure of human PCT was adapted from literature data [39]. Discovery Studio 4.0 was used for the preparation of protein for docking by removing the co-crystallized ligand, water molecules and co-factors [40]. To calculate Kollman charges and to add polar hydrogen, the AutoDockTools (ADT) graphical user interface was applied. Kaempferol was prepared for docking by minimizing its energy at the previously mentioned level of theory. The flexibility of the ligands was considered, while the protein or biomolecules remained as rigid structures in ADT. All kaempferol bonds were set to be rotatable. The Geistenger method for calculation of partial charges was employed. All calculations for protein–ligand flexible docking were performed using the Lamarckian Genetic Algorithm (LGA) method. A grid box with dimensions 92.007 Å × 0.202 Å × 0.111 Å of human PCT was used in order to cover the protein binding site and to enable the ligands to move freely. Inhibition potency of kaempferol was investigated and discussed.

4. RESULTS AND DISCUSSION

4.1. *Molecular geometry of kaempferol*

The structure of kaempferol (Fig. 1) was optimized using B3LYP-D3 functional. Due to the

lack of X-ray crystallographic structural data of pure kaempferol (to the best of our knowledge) the DAPK1-kaempferol complex (PDB code: 5AUX) structure was used [41], with the isolated parameters for the molecule of interest. Because of the rigidity of the molecule, it is expected that the structural parameters in the complex do not change significantly [42]. The most stable conformation of kaempferol was taken from our previous work [43, 44]. The calculated and experimental bond lengths are listed in Table 1.

Table 1 shows that B3LYP-D3 reproduces excellently the bond lengths of kaempferol with a mean correlation coefficient (R) of 0.991 and an average absolute error (AAE) for bond length of 0.012 Å. The optimized and experimental bond angles are given in Table S1 in the Supporting Information. The theoretical data indicate that kaempferol is planar (τ(C3–C2–C1`–C2`) is 0.0) (Table S1). On the other hand, the experimentally determined dihedral angle between B and C rings amounts to 168.9º.

T a b l e 1

The bond lengths in the neutral molecule, optimized with the B3LYP-D3/6-311++G(d,p) model (the atom numbering is in line with Figure 1). Experimental values are also included.

Bond length/Å	Kaempferol	
	Experimental	B3LYP
D(C2–O1)	1.365	1.373
D(C2–C3)	1.399	1.368
D(C2–C1`)	1.400	1.462
D(C3–C4)	1.391	1.450
D(C3–O3)	1.363	1.357
D(C4–C10)	1.391	1.434
D(C4–O4)	1.235	1.256
D(C10–C5)	1.398	1.422
D(C10–C9)	1.393	1.405
D(C5–C6)	1.392	1.387
D(C5–O5)	1.362	1.341
D(C6–C7)	1.391	1.402
D(C7–C8)	1.391	1.393
D(C7–O7)	1.363	1.360
D(C8–C9)	1.392	1.388
D(C9–O1)	1.369	1.358
D(Cl`–C2`)	1.394	1.407
D(C2`–C3`)	1.393	1.389
D(C3`–C4`)	1.394	1.396
D(C4`–C5`)	1.389	1.397
D(C4`–O4)	1.357	1.364
D(C5`–C6`)	1.391	1.384
D(Cl`–C6`)	1.390	1.410
D(O4`–H4`)	0.950	0.963
D(O3–H3)	0.950	0.976
D(O5–H5)	0.950	0.986
D(O7–H7)	0.950	0.963
D_H(O3–H3---O4)	/	2.032
D_H(O5–H5---O4)	1.718	1.777
R	0.991	
Average absolute error (AAE)	0.012	

D_H hydrogen bond

The deviation of the B ring from planarity is probably caused by the repulsion between H3 and H6` hydrogen atoms. If the known differences between the vacuum and condensed-phase environments are taken into the account, this discrepancy can be ascribed to the packing in the DAPK1–kaempferol complex (Fig. 2).

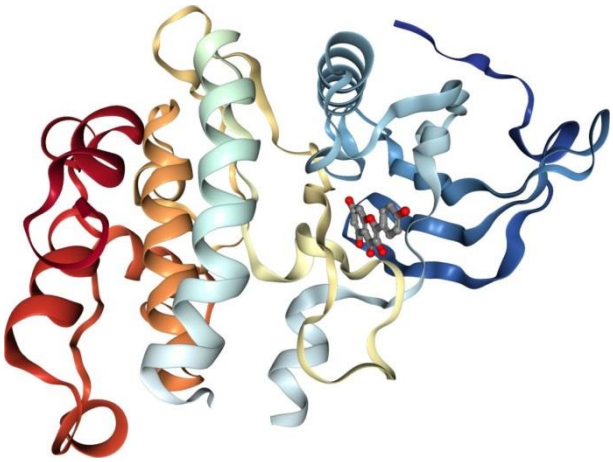

Fig. 2. Crystal structure of DAPK1–kaempferol complex (PDB code: 5AUX)

4.2. *NBO analysis*

The electronic structure of kaempferol was examined using NBO analysis. In order to evaluate the donor–acceptor interactions, analysis of the second-order Fock matrix was performed. The stabilization energy ($E^{(2)}$) for each donor (i) and acceptor (j) associated with the delocalization between i and j is determined as:

$$E^{(2)} = \Delta E_{ij} = q_i \frac{(F_{ij})^2}{\left(E_j - E_i\right)} \qquad (3)$$

where q_i is the donor orbital occupancy, E_i, E_j are the diagonal elements (orbital energies) and $F_{i,j}$ is the off-diagonal NBO Fock matrix element. The large $E^{(2)}$ value indicates the intensive interaction between the electron-donors and electron-acceptors and the greater extent of conjugation of the whole system. The possible intensive interactions are given in Table 2.

The most important interaction (n-π*) energy, related to resonance in the molecule, is electron donation from the LP2(O) atom orbitals to the antibonding acceptor π*(C–C) of the phenyl ring (LP2(O5) → π*(C5–C6) (159.2 kJ mol^{-1})). This large interaction energy indicates hyperconjugation between the electron-donating oxygen atom and the phenyl ring. Also, the other oxygen lone electron pairs show a significant electron-donating ability to the antibonding acceptor π*(C–C) orbital of the phenyl ring. Besides LP2(O) → π*(C–C) and LP2(O) → σ*(C–C) interactions, strong intramolecular hyperconjugative interactions are formed by orbital overlap between π(C–C) → π*(C–C) bond orbitals, resulting in intramolecular charge transfer (ICT), which causes stabilization of the system. These interactions lead to an increase in electron density (ED) in the C–C antibonding orbitals, which weakens their respective bonds. The EDs at the conjugated π(~1.63–1.76 e) and π* bonds (~0.3–0.4 e) of the phenyl and α-pyrone rings clearly demonstrate strong electron delocalization, leading to stabilization by ~43–144 kJ mol^{-1}.

The kaempferol structure is characterized by two intramolecular hydrogen bonds (IHBs) which additionally stabilize the structure. The NBO analysis revealed that the lone pair–antibonding orbital interactions between the carbonyl oxygen and the adjacent O–H bonds are responsible for the hydrogen-bond formation. Since the O4(2*p*) and O4(1*p*) orbitals are abundant in electrons, while the O5–H5(σ*) orbital is electron-deficient, it was found that charge transfer from the O4(2*p*) to the O5–H5(σ*) orbital is a favorable donor–acceptor interaction with stabilization energy of 57.61 kJ mol^{-1}. This has a significant effect on the strength of the hydrogen-bond delocalization energy. Also, there is significantly weaker charge transfer from O4(1*p*) to O5–H5(σ*) (Table 2). These findings are in accord with the IHB lengths, and the decrease in strength with bond elongation is proven (see Table 1). These are weaker interactions and the second-order interaction energies are proportional to the hydrogen-bond strengths.

The C2–C1′ bond length of about 1.462 Å (Table 1) lies between the bond lengths characteristic of aromatic and single C–C bonds, indicating weak electron delocalization between the B and C rings. This assumption is supported by the NBO analysis. A slightly greater *p*-orbital contribution to C1′ in the C2–C1′ bond (hybrid composition 0.710($sp^{1.66}$)C2 + 0.704($sp^{2.18}$)C1') could be the main reason for this bond being slightly longer than a double bond.

T a b l e 2

Second-order perturbation theory analysis of the kaempferol Fock matrix

Donor (*i*)	Acceptor (*j*)	ED (*i*)	ED (*j*)	$E^{(2)}$ kJmol^{-1}	E_i–E_j a.u.	$F_{i,j}$ a.u.
πC5-C6	π*C7-C8	1.69	0.40	116.9	0.28	0.08
πC5-C6	π*C9-C10	1.69	0.48	51.21	0.27	0.05
πC7-C8	π*C5-C6	1.66	0.36	53.09	0.28	0.05
πC7-C8	π*C9-C10	1.66	0.48	123.4	0.27	0.08
πC9-C10	π*C5-C6	1.63	0.36	102.8	0.29	0.08
πC9-C10	π*C7-C8	1.63	0.40	52.30	0.29	0.05
πC9-C10	π*O4-C4	1.63	0.41	143.8	0.26	0.09
πC2-C3	π*O4-C4	1.76	0.41	103.2	0.28	0.08
πC2-C3	π*C1`-C6`	1.76	0.40	43.30	0.32	0.05
πC1-C6`	π*C2-C3	1.63	0.31	78.62	0.27	0.06
πC1-C6`	π*C2`-C3`	1.63	0.30	90.00	0.28	0.07
πC1-C6`	π*C4`-C5`	1.63	0.39	73.30	0.27	0.06
πC2`-C3`	π*C1`-C6`	1.70	0.40	66.19	0.28	0.06
πC2`-C3`	π*C4`-C5`	1.70	0.39	95.31	0.27	0.07
πC4`-C5`	π*C1`-C6`	1.64	0.40	101.9	0.29	0.08
πC4`-C5`	π*C2`-C3`	1.64	0.30	64.10	0.29	0.06
LP1 O7	σ*C6-C7	1.98	0.02	24.60	1.16	0.07
LP2 O7	π*C7-C8	1.86	0.40	123.9	0.35	0.10
LP1 O5	σ*C5-C10	1.98	0.03	26.90	1.09	0.08
LP2 O5	π*C5-C6	1.82	0.36	159.2	0.33	0.11
LP1 O4	σ*H5-O	1.97	0.31	11.56	1.20	0.05
LP2 O4	σ*H5-O5	1.87	0.04	57.61	0.69	0.09
LP2 O4	σ*H3-O3	1.87	0.02	14.31	0.69	0.05
LP2 O4	σ*C4-C10	1.87	0.05	55.19	0.78	0.09
LP2 O4	σ*C3-C4	1.87	0.06	69.50	0.74	0.10
LP2 O1	π*C9-C10	1.76	0.48	125.9	0.36	0.10
LP2 O1	π*C2-C3	1.76	0.31	114.9	0.37	0.09
LP2 O3	π*C2-C3	1.87	0.31	124.4	0.34	0.09
LP1 O4`	σ*C4`-C5`	1.98	0.03	25.61	1.17	0.08
LP2 O4`	π*C4`-C5`	1.87	0.39	119.6	0.35	0.10

4.3. *Electrostatic potential and charge distribution*

The charge distribution in molecules is usually represented by a map of electrostatic potential (MEP). This is a useful feature to study reactive sites on the surface of the molecule, given that an approaching electrophile would be attracted to negative regions (electron-rich/red color) while the positive region (electron-poor/blue color) would be a preferred site for nucleophilic attack. MEP offers more intuitive way to understand the polarity of a molecule by correlating it with the molecular structure and the physicochemical properties [45–50]. The MEP of kaempferol is presented in Figure 3a.

The MEP in the case of the investigated molecule (Fig. 3a) clearly indicates that the chromene oxygen atom 4, as well as oxygen atoms 3, 5, 7 and 4′, contribute to the most electronegative regions (red). Due to the excess negative charge, one can expect a relatively high nucleophilic activity of this part of the molecule. This is in agreement with the fact that the negative regions of the MEP contain the electronegative atoms with the lone electron pairs. On the other hand, the positive MEP values are localized over the hydrogen atoms bonded to oxygen atoms.

The NBO analysis of the investigated compound was also performed. The obtained values of the natural charge distribution are presented in Figure 3b and are in accordance with MEP data. As expected, the negative charge is distributed mainly over the oxygen atoms attached to the benzene rings A and B as well as chromene ring C, while the rest of the negative natural charge is delocalized mostly over C6, C8, C10 in the A ring and over C atoms in the B ring.

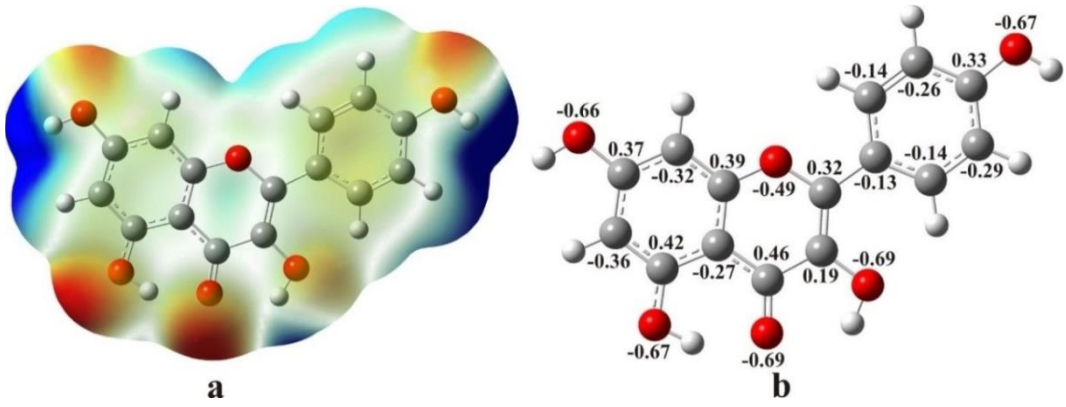

Fig. 3. Molecular electrostatic potential surface (left) and the natural charge distribution (right)

The C4 atom has greater positive charge than other C atoms in the chromene part of the molecule. In addition, the C5 atom has more positive value than other atoms in the A and B rings. On the other hand, a slightly positive natural charge is distributed almost uniformly over the hydrogen atoms. The obtained results indicate that the H atoms bonded to O7 and O4′ have more positive values than the other hydrogen atoms.

4.4. *Nonlinear optical activity*

The polarizabilities and the first-order hyperpolarizabilities of kaempferol were calculated using the DFT/B3LYP-D3 method with the 6-311++G (d,p) basis set in order to investigate the relationship between molecular structure and nonlinear optical properties (NLO). The calculated polarizability and the first hyperpolarizability (β) of kaempferol were based on the finite-field approach. The total electric dipole moment (μ), mean polarizability (Δα) and the total first-order static hyperpolarizability (β_{total}), were calculated using the x, y and z components of these electric moments [51]. It is well known that higher values of dipole moment, molecular polarizability and first-order hyperpolarizability are important for the more pronounced NLO properties of a compound. The calculated total electric dipole moment (μ), mean polarizability (α) and total first-order static hyperpolarizability (β_{total}) and their components are presented in Table S2. In the present case, the calculated total dipole moment of kaempferol is 1.78 D. The predicted value of the linear polarizability (α_{tot}) and total first-order static hyperpolarizability (β_{total}) are found to be 33.539×10^{-24} esu and 28.428×10^{-30} esu, respectively. The calculated value of β_{total} of kaempferol is 150 times higher than that of urea (0.1947×10^{-30} esu) [52], which is one of the prototypical molecules used in the study of the NLO properties of molecular systems and the value frequently used as a threshold for comparative purposes. Remarkably, the high polarizability of kaempferol shows its drug-likeliness as the high polarizability allows it to bind with its target very strongly.

4.5. *Vibrational spectra of kaempferol*

The experimentally obtained, theoretically calculated and scaled wavenumbers, with the assignments for the first 65 vibrational modes (of 87) in the region 3700–400 cm^{-1}, are presented in Table 3, together with the relative descriptions of IR and Raman intensities, PED values and the description of the largest vibrational contributions to the normal modes. The kaempferol geometry optimized in the gas phase served as the basis for calculation of the IR and Raman spectra using the B3LYP-D3/6–311++G(d,p) model. The B3LYP-D3/6–311++G(d,p)-calculated wavenumbers were corrected using a vibrational scaling factor value of 0.9873.

These calculated values are further discussed. The scaling factor was determined by the least-squares method, on the basis of the experimental data for the IR spectrum.

The most distinct bands in the IR spectrum of kaempferol are those in high-frequency region (4000–2000 cm^{-1}; Figure S1 in Supplementary Information) assigned to different modes of O–H and C–H vibrations. This region in the experimental spectrum is dominated by two overlapping and very strong-intensity bands, at 3420 and 3206 cm^{-1}. These intense bands could be taken as possible, different, absorptions by hydrogen bonds in kaempferol. This is the result confirmed by NBO analysis. Due to rather significant differences in wavenumber compared to the value predicted by DFT (3340 cm^{-1}, the scaled value) the experimentally obtained band at 3420 cm^{-1} is assigned to the O–H stretching vibration, mode 84 (Table 3).

T a b l e 3

Experimental and calculated positions of the bands in the IR and Raman spectra of kaempferol, with assignments and intensities of the normal modes

Mod	Assignments	Exp. values		B3LYP-D3/6-311++g(d,p)					
		IR cm^{-1}	Raman cm^{-1}	Unscaled freq. cm^{-1}	Scaled freq. cm^{-1}	IR intens.	Raman intens.	Raman scattering activities	PED (%)
87	OH stretching (A)			3832	3783	19	3	228	νOH (100)
86	OH stretching (B)			3830	3781	23	3	285	νOH(100)
85	OH stretching (C)			3619	3573	26	2	191	νOH(100)
84	OH stretching (A)	3420 vs		3383	3340	60	2	126	νOH(99)
83	CH stretching (B)	3206 s		3243	3202	1	0	30	νCH(99)
82	CH stretching (A)			3223	3182	0	1	71	νCH(100)
81	CH stretching (B)			3218	3177	0	1	57	νCH(91)
80	CH stretching (B)			3191	3151	1	2	129	νCH(91)
79	CH stretching (A)			3181	3140	1	3	192	νCH(100)
78	CH stretching (B)			3155	3115	4	3	165	νCH(99)
77	C=O stretching (C) C2=C3 stretching (C) CC stretching (A,C)	1660 vs		1685	1663	76	24	563	νCO(30) + νCC(20)
76	C=C stretching (B,C)		1642 m	1661	1640	13	8	191	νCC(63)
75	CC stretching (B,C) HCC bending (B) C=O stretching (C)			1647	1626	46	100	2276	νCC(50) + δHCC(11) + νCO(10)
74	C=O stretching (C) CC stretching (A,C)	1612 vs	1604 vs	1631	1610	100	6	130	νCO(49) + νCC(12)
73	CC stretching (B)			1617	1596	0	0	5	νCC(63)
72	C2=C3stretching (C) CC stretching (A,C) C=O stretching (C)	1568 m	1561 m	1596	1576	26	35	762	νCC(50) + νCO(14)
71	HCC bending (B) HOC bending (B,C)			1545	1526	20	7	137	δHCC(25) + δHOC(24)
70	CC stretching (A,C)	1509 s	1509 w	1530	1511	64	5	108	νCC(12) + δCCO(11) + δHOC(10) + δHCC(10) + δCCC(10)
69	CC stretching (A,C) HCC bending (A) HOC bending (A,C) C=O stretching (C)			1506	1487	38	5	92	νCC(40) + νCO(12)
68	CC stretching (A,C) COH bending (A) CCH bending (A) CO stretching (C)	1456 vw		1470	1452	15	15	293	νCC(28) + δHCC(20) + δHOC(17)
67	CC stretching (A,C) COH bending (A,C) CCH bending (A) CO stretching (C)	1440 vw	1422 w	1452	1434	7	13	243	νCC(10) + δHCC(10) + δHOC(10)
66	CC stretching (A) HOC bending (A,B,C) HCC bending (A,B)			1424	1405	13	9	174	νCC(40) + δHOC(14) + δHCC(10)
65	CC stretching (A,C) CO stretching (C) COH bending (A,C)	1382 s		1396	1378	28	3	49	νCO(17) + νCC(17) + δCCC(11)
64	CC stretching (A,C) CO stretching (A,C) COH bending (B) CCH bending (B)		1366 w	1376	1358	2	1	17	δHCC(48) + δHOC(12) + νCC(21)
63	CO stretching (A,C) HOC bending (A,C) HCC bending (A,B) CC stretching (A)			1351	1333	27	8	137	νCO(35) + νCC(25)

Table 3 continuation

62	CC stretching (A,C) CO stretching (A,C) COH bending (C,B)	1316 m		1343	1326	57	43	747	νCC(21) + δHOC(18) + νCO(10)
61	CO stretching (A,B,C) HOC bending (A,B,C) HCC bending (B) CCC bending (C,B)	1306 m	1316 w	1332	1315	10	0	7	νCC(40) + δHCC(19) + νCO(11)
60	CC stretching (B) CO stretching (A,C) HOC bending (B) HCC bending (B)	1275 vw	1277 w	1295	1278	27	4	71	νCO(35) + δHCC(17) + νCC(16)
59	CO stretching (A,C) CC stretching (A)			1281	1264	32	1	22	νCO(25) + νCC(24)
58	CC stretching (A,C) CO stretching (A,C) HOC bending (A) HCC bending (A) COC bending (C)	1252 m		1259	1243	8	1	15	νCO(22) + δHCC(20) + δHOC(20)
57	HCC bending (A,B) CCC bending (A,B,C) HOC bending (C) CCO bending (C) COC bending (C)	1223 m	1222 w	1227	1211	32	0	3	νCO(37) + δHCC(10)
56	CO stretching (C) HOC bending (A,B,C) HCC bending (A,B)			1210	1195	18	17	263	δHCC(48) + νCO(24)
55	CCO bending (A,C) COH bending (A,C) HCC bending (A)		1185 m	1197	1182	9	2	29	νCO(25) + δHCC(14) + δHOC(13)
54	HOC bending (A,B) HCC bending (B)			1189	1174	46	5	77	δHOC(40) + δHCC(30)
53	COH bending (A) CCH bending (A)	1177 vs		1176	1161	74	2	24	δHCC(25) + δHOC(23)
52	CCH bending (A,B) COH bending (C,B)			1152	1137	3	1	11	νCO(38) + δHOC(16) + δHCC(15)
51	COH bending (A,B,C) CCH bending (A,B)	1129 vw	1117 vw	1138	1123	9	1	9	νCO(20) + δHCC(13) + δHOC(11) + δCCC(10)
50	CCH bending (A,B) COH bending (A,C) COC bending (C) CCC bending (A,B,C)	1090 w	1090 vw	1103	1089	4	1	16	νCO(30) + δHCC(14) + δHOC(10) + δCCC(10)
49	HCC bending (A,B) CCC bending (B)			1030	1017	2	1	7	δHCC(43) + δCCC(42)
48	CCH bending (A) COH bending (A,C)	1008 w	1008 vw	1023	1010	4	0	5	νCO(45) + δHCC(42)
47	CCH bending (A) COH bending (A,C)	974 w	976 vw	991	978	6	4	50	νCO(40) + δHCC(15) + δCCC(11)
46	HCCC torsion (B)			985	972	0	0	0	τHCCC(90)
45	HCCC torsion (B)			965	953	0	0	0	τHCCC(90)
44	CCC bending (A,B,C) CCO bending (A,C) COH bending (A,B,C) CCH bending (A,B)		882 vw	892	881	3	0	3	δHCC(14) + δCCC(14) + δCOC(11) + δCCO(11) + δHOC(10)
43	HCCC torsion (B)			850	839	9	0	0	τHCCC(90)
42	CCO bending (A,B,C) COH bending (B) CCC bending (B) CCH bending (A,B)		828 vw	834	823	3	8	77	νCO(24) + δCCC(20) + δCCO(18)
41	HCCC torsion (A) HOCC torsion (A)			826	816	0	0	0	τHCCC(50) + τHOCC(40)
40	HCCC torsion (A,B)			820	809	0	0	0	τHCCC(93)
39	HCCC torsion (A,B) HOCC torsion (A)			818	808	7	0	0	τHCCC(45) + τHOCC(37)
38	HOCC torsion (A)			776	766	22	0	1	ττHOCC(79)

Table 3 continuation

37	HCCC torsion (A,B) HOCC torsion (A) OCCC torsion (C) o.p. CCCC torsion (C,B)		725 vw	728	718	0	0	3	τHCCC(26) + τHOCC(20) + γOCCC(15) + τCCCC(10)
36	HCCC torsion (A,B) HOCC torsion (A) OCCC torsion (C) o.p. CCCC torsion (C,B)			726	717	0	0	2	τHCCC(28) + τHOCC(23) + γOCCC(15) + τCCCC(15)
35	CCO bending (A,C) CCC bending (A,B,C) COC bending (C) HCC bending (A,B)			722	713	0	0	1	δCCO(17) + δCCC(15) + δCOC(14) + δHCC(12)
34	CCO bending (A,B,C) COC bending (C) CCC bending (A,B,C)	702 vw	690 w	692	683	2	2	14	δCCC(18) + δCCO(15) + δHCC(10)
33	HCCC torsion (A,B) CCCC torsion (A) HOCC torsion (A)			679	670	0	0	0	τHCCC(35) + τCCCC(28) + τHOCC(24)
32	CCC bending (B) HCC bending (B)			653	645	0	1	6	δCCC(60) + δHCC(27)
31	CCO bending (A) CCC bending (A,B,C) COC bending (C)	639 vw	637 w	644	636	3	3	20	δCCC(15) + δCCO(14) + δHCC(14)
30	CCO bending (B)	620 vw		640	632	1	0	2	τHCCC(17) + τCCOC(18) + τCCCC(17)
29	HCCC torsion (A,B) HOCC torsion (A,C) COCC torsion (C) CCCC torsion (B,C)			626	618	0	0	1	τHCCC(23) + τHOCC(20) + τCOCC(19) + τCCCC(14)
28	HCCC torsion (A,B) HOCC torsion (A,C) CCCO torsion (A)			603	596	1	0	0	τHCCC(30) + τHOCC(25) + τCCCO(20)
27	CCOH torsion (A,B) CCCO torsion (A,B,C) CCOC torsion (C) CCCC torsion (B)	584 vw	578 vw	589	582	3	7	45	δCCC(15) + δCCO(13) + δHCC(12) + δHOC(12) + νCO(10)
26	CCOH torsion (A,B,C) CCOC torsion (C) CCCC torsion (A,B,C)	565 vw	565 w	572	565	5	1	7	δCCO(20) + δHCC(17) + δHOC(17) + δCCC(14)
25	CCCH torsion (A) CCCC torsion (A) CCOH torsion (A) HCCO torsion (A,C)		516 vw	528	521	2	2	13	δCCO(20) + δCCC(17) + δHCC(15) + δHOC(15) + δCOC(12)
24	HOCC torsion (B,C) HCCC torsion (B)			502	496	1	0	1	τHOCC(44) + τHCCC(33)
23	CCCH torsion (A,B) CCCC torsion (A,C) CCOH torsion (A) HCCO torsion (A,C)		460 vw	462	456	0	1	5	δCCO(17) + δCCC(16) + δHCC(14) + δHOC(13) + δCOC(11)

The high-frequency region is characteristic of C–H stretching modes of the A and B rings as well. In the 4000–3000 cm^{-1} Raman region (Figure S2) there are no bands easily assignable to the O–H and C–H stretching modes. The vibrational contributions to the normal modes (PED values in Table 3) in the 3780–3115 cm^{-1} region are assigned solely to the O–H and C–H stretching modes themselves (91–100%). The remaining modes are presented as combinations of the various contributions.

The majority of the medium-to-strong-intensity bands in both IR and Raman spectra of kaempferol are to be found in the 1800–1500 cm^{-1} region (Figs. 4 and 5, Table 3). This region involves combinations of the C=O stretching ($1660_{(IR)}$, $1612_{(IR)}$ and $1604_{(R)}$ cm^{-1}; modes ν_{77} and ν_{74}), C2=C3 stretching ($1660_{(IR)}$ and $1568_{(IR)}$ cm^{-1} and $1561_{(R)}$ cm^{-1}; modes ν_{77} and ν_{72}) and C–C stretching ($1660_{(IR)}$,$1612_{(IR)}$, $1568_{(IR)}$, $1509_{(IR)}$ cm^{-1}, $1642_{(R)}$, $1604_{(R)}$, $561_{(R)}$ and $1509_{(R)}$ cm^{-1}; modes ν_{77}, ν_{74}, ν_{72} and ν_{70}) modes.

In the region between 1500 and 1000 cm^{-1}, bands mostly involve C–C stretching, O–C stretching and in-plane C–C–H, C–O–H, C–C–O and C–C–C bending vibrations of the rings. The medium-to-strong-intensity bands in the same region belong to modes at $1382_{(IR)}$, $1316_{(IR)}$, $1306_{(IR)}$, $1252_{(IR)}$, $1223_{(IR)}$ and $1185_{(R)}$ cm^{-1} (modes ν_{65}, ν_{62}, ν_{61}, ν_{58},

$\nu_{57,}$ and $\nu_{53,}$ respectively) (Figs. 4 and 5, Table 3). The low- (and very low-) intensity bands observed at $1456_{(IR)}$, $1440_{(IR)}$, $1442_{(R)}$, $1366_{(IR)}$, $1316_{(R)}$, $1275_{(IR)}$, $1277_{(R)}$, $1222_{(R)}$, $1129_{(IR)}$, $1117_{(R)}$, $1090_{(IR, R)}$ and $1008_{(IR, R)}$, cm^{-1} (modes ν_{68}, ν_{67}, ν_{64}, ν_{61}, ν_{60}, ν_{57}, ν_{51}, ν_{50} and ν_{48}) are also assigned to the different stretching (C–C, O–C) and bending (C–C–H, C–O–H, C–C–O, C–C–C) modes of the rings.

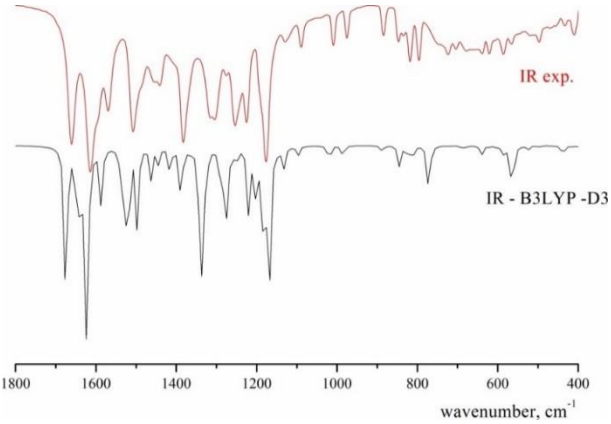

Fig. 4. The 1800–400 cm^{-1} IR regions of the experimental and theoretical spectra of kaempferol

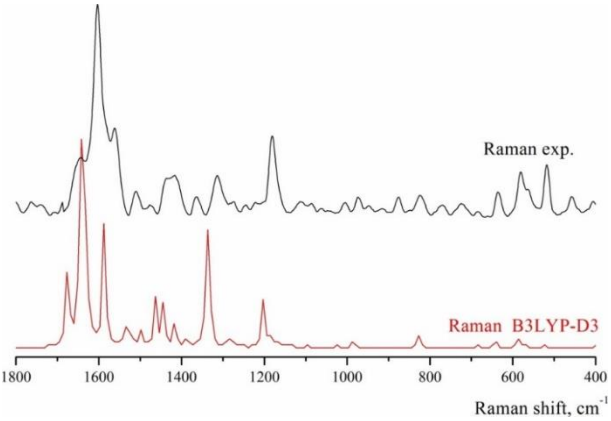

Fig. 5. The 1800–400 cm^{-1} Raman regions of the experimental and theoretical spectra of kaempferol

The linear relationship between the experimental and calculated wavelengths was proven from the data presented in Table 3. Three descriptors: the correlation coefficient (R), the average absolute error (AAE), and the average relative error (ARE), were used to examine the quality of the linear correlation. The R values for the IR and Raman spectra are 0.9999 and 0.9997. The AAE and ARE values for the IR spectrum are 11 cm^{-1} and 1.0%, while for the Raman spectrum these values are 7 cm^{-1} and 0.7%. According to the obtained results, the B3LYP-D3 functional can be considered as giving very good agreement between the experimentally and theoretically obtained spectra.

4.6. *NMR spectra of kaempferol*

The ^{13}C and ^{1}H NMR spectra of kaempferol were measured in DMSO and used to confirm the structure of the molecule. The experimental results were compared to the theoretical values determined by the GIAO method. The scaling factor of 0.932 (^{1}H NMR) was determined by the least-squares method. The experimental and theoretical positions of the peaks in the ^{13}C NMR and ^{1}H NMR spectra are given in Tables 4 and 5. The corresponding spectra are presented in Figures S3 and S4 (the atom numbering is in line with the designation in Fig. 1).

T a b l e 4

Calculated and experimental ^{13}C NMR chemical shifts of the selected carbons

^{13}C NMR	Experimental	Calculated
C(2)	147.0	146.2
C(3)	135.8	135.1
C(4)	176.0	175.1
C(5)	160.9	160.0
C(6)	103.2	102.7
C(7)	164.1	163.3
C(8)	93.7	93.2
C(9)	156.4	155.6
C(10)	98.4	97.9
C(1`)	121.8	121.2
C(2`)	129.6	129.0
C(3`)	115.6	115.0
C(4`')	159.3	158.5
C(5`)	115.6	115.0
C(6`)	129.6	129.0
Average absolute error (AAE)		0.68
R		0.999

T a b l e 5

Calculated and experimental ^{1}H NMR chemical shifts of the protons bonded to carbons

^{1}H NMR	Experimental	Calculated
C(6)H	6.19	6.21
C(8)H	6.44	6.35
C(2`)H	8.09	8.37
C(3`)H	6.92	6.80
C(5`)H	6.92	6.93
C(6`)H	8.09	7.96
Average absolute error (AAE)		0.11
R		0.986

The chemical shifts obtained experimentally are in the perfect agreement with the available literature data (R = 1.0000) [42, 53]. The calculated and experimental chemical shift values given in Tables 4 and 5 show good correspondence. The correlation coefficients in Tables 4 and 5 are moderately large, while the AAEs are relatively small. According to the values of R and AAE, B3LYP-D3 shows a reasonable ability to describe the NMR parameters of kaempferol.

4.7. *Molecular docking studies*

To evaluate the inhibitory nature of kaempferol against human PCT, a molecular docking investigation was performed. Protein–ligand binding energy and identification of the potential ligand binding sites were also determined from this study. The ligand conformation that showed the lowest binding energy (best position) was determined based on the ligand docking results. The position and orientation of ligand inside the protein receptor and the interactions with amino acids, which are bound to the ligand, were analyzed and visualized with Discovery Studio 4.0 and AutoDockTools.

Table S3 gives the values of the estimated free energy of binding and inhibition constants (K_i), for the investigated ligand in 10 different conformations. Lower values of K_i indicate better inhibition. The lowest values of ΔG_{bind} and K_i are found for conformation 1 (Table S3). Based on analysis of the relative positions of the ligand and the active amino acids, it can be concluded that the ligand binds to the catalytic site of the substrate by weak non-covalent interactions. The most prominent are H-bonds and alkyl–π interactions. ASP in position 53 in the primary structure of the PCT chain has a predominant role as the active site of human PCT regarding its inhibition action. This result stands regardless of the conformation of the investigated ligand (Fig. 6). ASP53 forms one H-bond (2.27 Å length) with an O-H group of the ligand (Fig. 6). PRO55, ARG56 and LEU52 form weak alkyl–π interactions with the benzene and chromene rings of the ligand (Fig. 6).

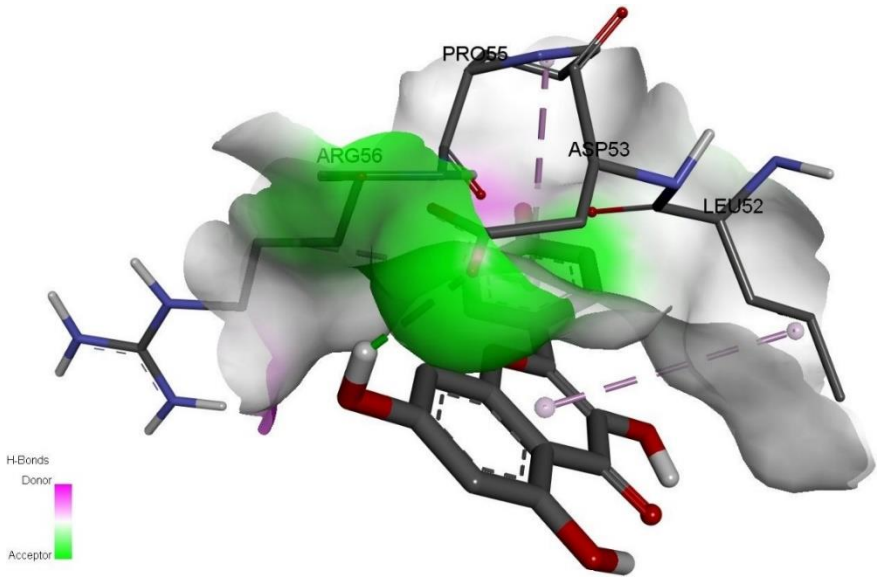

Fig. 6. Interactions between ligand (conformation 1, the lowest K_i) and amino acids in procalcitonin

5. CONCLUSIONS

The results of the application of the B3LYP-D3/6-311++G(d,p) density functional method in determination of the spectroscopic and electronic features of kaempferol point to a planar molecule, characterized by the facilitated electron delocalization between the B and C rings. Three IR and Raman spectra descriptors (the correlation coefficient R, the average absolute error AAE, and the average relative error ARE) demonstrate that B3LYP-D3 provides very good agreement between the experimental and simulated vibrational spectra. Two NMR spectral descriptors (R and AAE) indicate the B3LYP-D3 method as showing reasonably good results in describing the NMR spectrum of kaempferol. The calculated high polarizability value of kaempferol indicates the possibility of its tight binding to the biologically active components. The results of molecular docking study have shown that kaempferol, when acting as the ligand, can form a stable complex with human procalci-

tonin protein, as evidenced by the binding energy value (ΔG_{bind} = –2.68 kcal mol^{-1}). The most important interactions are H-bonds and alkyl–π interactions. These preliminary results suggest that kaempferol might exhibit significant inhibitory activity against PCT.

Acknowledgements. The authors acknowledge financial support by the Ministry of Education, Science and Technological Development of the Republic of Serbia (Grants No. 172015 and 172040). The authors thank Prof. Jamróz MH for the VEDA 4 software.

REFERENCES

[1] V. Cody, E. Middleton, J. B. Harborne, Plant flavonoids in biology and medicine. Biochemical, pharmacological, and structure-activity relationships. Proceedings of a symposium, Buffalo, New York, July 22–26, 1985, *Prog. Clin. Biol. Res.* **213,** 1–592 (1986).

[2] C. Rice-Evans, Flavonoid antioxidants, *Curr. Med. Chem.* **8,** 797–807 (2001). DOI:10.2174/0929867013373011

[3] J. M. Calderón-Montaño, E. Burgos-Morón, C. Pérez-Guerrero, M. López-Lázaro, A review on the dietary flavonoid kaempferol, *Mini Rev. Med. Chem.* **11,** 298–344 (2011). DOI:10.2174/138955711795305335.

[4] S. V. Jovanovic, S. Steenken, M. Tosic, B. Marjanovic, M. G. Simic, Flavonoids as antioxidants, *J. Am. Chem. Soc.* **116,** 4846–4851 (1994). DOI**:**10.1021/ja00090a032.

[5] P. G. Pietta, Flavonoids as antioxidants, *J. Nat. Prod.* **63,** 1035–1042 (2000). DOI:10.1021/np9904509.

[6] A. Marfak, P. Trouillas, D. P. Allais, Y. Champavier, C. A. Calliste, J. L. Duroux, Radiolysis of kaempferol in water/methanol mixtures. Evaluation of antioxidant activity of kaempferol and products formed, *J. Agric. Food Chem.* **51,** 1270–1277 (2003). DOI:10.1021/jf020836g.

[7] T. Walle, Absorption and metabolism of flavonoids, *Free Rad. Biol. Med.* **36,** 829–837 (2004). DOI:10.1016/j.freeradbiomed.2004.01.002.

[8] R. J. Williams, J. P. E. Spencer, C. Rice-Evans, Flavonoids: antioxidants or signalling molecules? *Free Rad. Biol. Med.* **36,** 838–849 (2004). DOI:10.1016/j.freeradbiomed.2004.01.001.

[9] C. G. Fraga, M. Galleano, S. V. Verstraeten, P. I. Oteiza, Basic biochemical mechanisms behind the health benefits of polyphenols, *Mol. Aspects Med.* **31,** 435–445 (2010). DOI:10.1016/j.mam.2010.09.006.

[10] R. M. Han, J. P. Zhang, L. H. Skibsted, Reaction dynamics of flavonoids and carotenoids as antioxidants, *Molecules* **17,** 2140–2160 (2012). DOI:10.3390/molecules17022140.

[11] D. Pal, P. Verma, Flavonoids: a powerful and abundant source of antioxidants, *Int. J. Pharm. Pharm. Sci.* **5**, 95–98 (2013).

[12] D. Procházková, I. Boušová, N. Wilhelmová, Antioxidant and prooxidant properties of flavonoids, *Fitoterapia* **82,** 513–523 (2011). DOI:10.1016/j.fitote.2011.01.018.

[13] J. B. Harborne, H. Baxter, *The Handbook of Natural Flavonoids*, John Wiley & Sons, Chichester, New York, 1999.

[14] J. Heilmann, I. Merfort, M. Weiss, Radical scavenger activity of different 3',4'-dihydroxyflavonols and 1,5-dicaffeoylquinic acid studied by inhibition of chemiluminescence, *Planta Med.* **61,** 435–438 (1995). DOI:10.1055/s-2006-958131.

[15] A. Galano, G. Mazzone, R. Alvarez-Diduk, T. Marino, J. R. Alvarez-IdaboyR, N. Russo, Food antioxidants: chemical insights at the molecular level, *Annu. Rev. Food Sci. Technol.* **7,** 335–352 (2016). DOI:10.1146/annurev-food-041715-033206.

[16] M. Leopoldini, N. Russo, M. Toscano, The molecular basis of working mechanism of natural polyphenolic antioxidants, *Food Chem.* **125,** 288–306 (2011). DOI:10.1016/j.foodchem.2010.08.012.

[17] Ø. M. Andersen, K. R. Markham, *Flavonoids: Chemistry, Biochemistry and Applications*, Taylor and Francis, Boca Raton, New York, 2006.

[18] P. Rajendran, T. Rengarajan, N. Nandakumar, R. Palaniswami, Y. Nishigaki, I. Nishigaki, Kaempferol, a potential cytostatic and cure for inflammatory disorders, *Eur. J. Med. Chem.* **86,** 103–112 (2014). DOI:10.1016/j.ejmech.2014.08.011.

[19] U. Çoruh, R. Ustabaş, H. Türker Akçay, E. Menteşe, E. M. Vazquez Lopez, Experimental and theoretical studies of 4-[(4-methyl-5-phenyl-4H1,2,4-triazol-3-zl)sulfanyl] benzene-1,2-dicarbonitrile, *Maced. J. Chem. Chem. Eng.* **35**, 165–177 (2016). DOI:10.20450/mjcce.2016.836.

[20] M. A. Al-Alshaikh, S. Muthu, E. S. Al-Abdullah, E. E. Porchelvi, S. Lahsasni, A. A. El-Emam, Structural and spectroscopic characterization of N′-[(1*E*)-(4-fluorophenyl)methylidene]thiophene-2-carbohydrayide, *Maced. J. Chem. Chem. Eng.* **35,** 63–77 (2016). DOI:10.20450/mjcce.2016.811.

[21] R. Álvarez-Diduk, M. T. Ramírez-Silva, A. Galano, A. Merkoçi, Deprotonation mechanism and acidity constants in aqueous solution of flavonols: a combined experimental and theoretical study, *J. Phys. Chem. B* **117,** 12347–12359 (2013). DOI:10.1021/jp4049617.

[22] W. Weglöhner, J. Struck, C. Fischer-Schulz, N. G. Morgenthaler, A. Otto, C. Bohuon, A. Bergmann, Isolation and characterization of serum procalcitonin from patients with sepsis, *Peptides* **22,** 2099–2103 (2001).

[23] E. S. Nylén, R. H. Snider Jr, K. A. Thompson, P. Rohatgi, K. L. Becker, Pneumonitis-associated hyperprocalcitoninemia, *Am. J. Med. Sci.* **312,** 12–18 (1996). DOI:10.1016/S0002-9629(15)41740-9.

[24] R. Wysokiński, K. Hernik, R. Szostak, D. Michalska, Electronic structure and vibrational spectra of *cis*-diammine(orotato)platinum(II), a potential cisplatin analogue: DFT and experimental study, *Chem Phys.*, **333**:37–48, 2007.

[25] A. D. Becke, Density-functional exchange-energy approximation with correct asymptotic behavior, *Phys. Rev. A* **38,** 3098–3100 (1988). DOI:10.1103/PhysRevA.38.3098.

[26] A. D. Becke, Density-functional thermochemistry. III. The role of exact exchange, *J. Chem. Phys.* **98,** 648–5652 (1993). DOI:10.1063/1.464913.

[27] A. D. Becke, E. R. Johnson, A density-functional model of the dispersion interaction, *J. Chem. Phys.* **123**, 154101–154103 (2005). DOI:10.1063/1.2065267.

[28] M. J. Frisch, G. W. Trucks, H. B. Schlegel, G. E. Scuseria, M. A. Robb, J. R. Cheeseman, G. Scalmani, V.

Barone, B. Mennucci, G. A. Petersson, H. Nakatsuji, M. Caricato, X. Li, H. P. Hratchian, A. F. Izmaylov, J. Bloino, G. Zheng, J. L. Sonnenberg, M. Hada, M. Ehara, K. Toyota, R. Fukuda, J. Hasegawa, M. Ishida, T. Nakajima, Y. Honda, O. Kitao, H. Nakai, T. Vreven, J. A. Montgomery, Jr., J. E. Peralta, F. Ogliaro, M. Bearpark, J. J. Heyd, E. Brothers, K. N. Kudin, V. N. Staroverov, T. Keith, R. Kobayashi, J. Normand, K. Raghavachari, A. Rendell, J. C. Burant, S. S. Iyengar, J. Tomasi, M. Cossi, N. Rega, J. M. Millam, M. Klene, J. E. Knox, J. B. Cross, V. Bakken, C. Adamo, J. Jaramillo, R. Gomperts, R. E. Stratmann, O. Yazyev, A. J. Austin, R. Cammi, C. Pomelli, J. W. Ochterski, R. L. Martin, K. Morokuma, V. G. Zakrzewski, G. A. Voth, P. Salvador, J. J. Dannenberg, S. Dapprich, A. D. Daniels, O. Farkas, J. B. Foresman, J. V. Ortiz, J. Cioslowski, and D. J. Fox, *Gaussian 09, Revision D.01* Gaussian, Inc.: Wallingford, CT, 2010.

[29] M. Sardo, R. Siegel, S. M. Santos, J. Rocha, J. R. B. Gomes, L. Mafra, Combining multinuclear high-resolution solid-state MAS NMR and computational methods for resonance assignment of glutathione tripeptide, *J. Phys. Chem. A* **116,** 6711–6719 (2012). DOI:10.1021/jp302128r.

[30] P. Ivanov, Performance of some DFT functionals with dispersion on modeling of the translational isomers of a solvent-switchable [2]rotaxane, *J. Mol. Struct.* **1107,** 31–38 (2016). DOI:10.1016/j.molstruc.2015.11.015.

[31] S. Grimme, S. Ehrlich, L. Goerigk, Effect of the damping function in dispersion corrected density functional theory, *J. Comp. Chem.* **32,** 1456–1465 (2011). DOI:10.1002/jcc.21759.

[32] S. Grimme, J. Antony, S. Ehrlich, H. Krieg, A consistent and accurate ab initio parametrization of density functional dispersion correction (DFT-D) for the 94 elements H-Pu, *J. Chem. Phys.* **132,** 154104–154107 (2010). DOI:10.1063/1.3382344.

[33] R. A. Munos, Y. N. Panchenko, G. S. Koptev, N. F Stepanov, Program for calculating distribution of potential energy in internal coordinates, *J. Appl. Spectrosc.* **12,** 428–429 (1970).

[34] M. H. Jamróz, Vibrational energy distribution analysis *VEDA 4*, Warsaw, 2004.

[35] K. Wolinski, J. F. Hinton, P. Pulay, Efficient implementation of the gauge-independent atomic orbital method for NMR chemical shift calculations, *J. Am. Chem. Soc.* **112,** 8251–8260 (1990). DOI:10.1021/ja00179a005.

[36] J. E. Carpenter, F. Weinhold, Analysis of the geometry of the hydroxymethyl radical by the "different hybrids for different spins" natural bond orbital procedure, *J. Mol. Struct. THEOCHEM* **169,** 41–62 (1988).

[37] A. E. Reed, L. A. Curtiss, F. Weinhold, Intermolecular interactions from a natural bond orbital, donor-acceptor viewpoint, *Chem. Rev.* **88,** 899–926 (1988). DOI:10.1021/cr00088a005.

[38] G. M. Morris, R. Huey, W. Lindstrom, M. F. Sanner, R. K. Belew, D. S. Goodsell, A.J. Olson, AutoDock4 and AutoDockTools4: Automated docking with selective receptor flexibility, *J. Comput. Chem.* **30,** 2785–2791 (2009). DOI:10.1002/jcc.21256.

[39] J. M. Le Moullec, A. Jullienne, J. Chenais, F. Lasmoles, J. M. Guliana, G. Milhaud, M. S. Moukhtar, The complete sequence of human preprocalcitonin, *FEBS Lett.* **167,** 93–97 (1984). DOI:10.1016/0014-5793(84)80839-X.

[40] *BIOVIA Discovery Studio v4.0*, Accelrys Software, Inc., San Diego, 2016.

[41] T. Yokoyama, Y. Kosaka, M. Mizuguchi, Structural insight into the interactions between death-associated protein kinase 1 and natural flavonoids, *J. Med. Chem.* **58,** 7400–7408 (2015). DOI:10.1021/acs.jmedchem.5b00893.

[42] R. Zieliński, H. Szymusiak, Application of DFT B3LYP/GIAO and B3LYP/CSGT methods for interpretation of NMR spectra of flavonoids, *Pol. J. Food Nutr. Sci.* **12,** 157–162 (2003).

[43] J. M. Dimitrić Marković, D. Amić, B. Lučić, Z. S. Marković, Oxidation of kaempferol and its iron(III) complex by DPPH radicals: spectroscopic and theoretical study, *Monatsh. Chem.* **145,** 557–563 (2014). DOI:10.1007/s00706-013-1135-z.

[44] J. M. Dimitrić Marković, D. Milenković, D. Amić, A. Popović-Bijelić, M. Mojović, I. A. Pašti, Z. S. Marković, Energy requirements of the reactions of kaempferol and selected radical species in different media: towards the prediction of the possible radical scavenging mechanisms, *Struct. Chem.* **25,** 1795–1804 (2014). DOI:10.1007/s11224-014-0453-z.

[45] J. S. Murray, K. D. Sen, *Molecular Electrostatic Potentials : Concepts and Applications*, Elsevier, Amsterdam, 1996.

[46] I. Alkorta, J. J. Perez, Molecular polarization potential maps of the nucleic acid bases, *Int. J. Quantum Chem.* **57,** 123–135 (1996). DOI:10.1002/(sici)1097-461x(1996)57:1<123::aid-qua14>3.0.co;2-9.

[47] E. Scrocco, J. Tomasi, Electronic molecular structure, reactivity and intermolecular forces: A heuristic interpretation by means of electrostatic molecular potentials, *Adv. Quantum Chem.* **11,** 116–193 (1978).

[48] F. J. Luque, M. Orozco, P. K. Bhadane, S. R. Gadre, SCRF calculation of the effect of water on the topology of the molecular electrostatic potential, *J. Phys. Chem.* **97,** 9380–9384 (1993). DOI:10.1021/j100139a021.

[49] J. Šponer, P. Hobza, DNA base amino groups and their role in molecular interactions: Ab initio and preliminary density functional theory calculations, *Int. J. Quantum Chem.* **57,** 959–970 (1996). DOI:10.1002/(SICI)1097-461X(1996)57:5<959::AID-QUA16>3.0.CO;2-S.

[50] S. R. Gadre, I. H. Shrivastava, Shapes and sizes of molecular anions via topographical analysis of electrostatic potential, *J. Chem. Phys.* **94,** 4384–4390 (1991). DOI:10.1063/1.460625.

[51] D. M. Burl, R. D. Miller, C. A. Walsh, Second-order nonlinearity in poled-polymer systems, *Chem. Rev.* **94,** 31–75 (1994). DOI:10.1021/cr00025a002.

[52] C. Adant, M. Dupuis, J. L. Bredas, Ab initio study of the nonlinear optical properties of urea: Electron correlation and dispersion effects, *Int. J. Quantum Chem.* **56,** 497–507 (1995). DOI:10.1002/qua.560560853.

[53] M. Sikorska, I. Matławska, Kaempferol, isorhamnetin and their glycosides in the flowers of Asclepias syriaca L, *Acta Pol. Pharm.* **58,** 269–272 (2001).